Supporting Information

Plasma-Treated 1D Transition Metal Dichalcogenides for Efficient Electrocatalytic Hydrogen Evolution Reaction

Asmita Dutta[a], Manjunath Krishnappa[b,c], Hani Porat[a], Ronit Lavi[d], Aneena Lal[a], Manish Kumar Yadav[a], Vilko Mandić[e], Gennady Makrinich[b], Alex Laikhtman[b], Alla Zak[b], Arie Borenstein[a]*

a- Department of Chemical Sciences, Ariel University, Ariel, Israel

b- Department of Physics, the Faculty of Sciences, Holon Institute of Technology (HIT), Holon, Israel

c- Department of Chemistry, Advanced Research Centre for Clean and Green Energy, Nitte Meenakshi Institute of Technology, Bangalore, India

d- Department of Chemistry, Bar Ilan University, Ramat Gan, Israel

e- Faculty of Chemical Engineering and Technology, University of Zagreb, Zagreb, Croatia

*- corresponding author. Email: arieb@ariel.ac.il

Table of Contents
Tables

Tables

Table S1: FWHM (full-width half maximum) of (002) plane from the XRD peaks and crystallite size for pristine WS_2 NTs and plasma treated WS_2 NTs.

	FWHM (full-width half maximum)	Crystallite Size (Å)
WS_2	0.475	2.94
WS_2-Ar	0.477	2.92
WS_2-D_2	0.478	2.92
WS_2-Ar-D_2	0.482	2.89

Table S2. Atomic percentages calculated from XPS data for pristine and plasma-treated WS_2 NTs samples.

Elements	WS_2	WS_2-Ar	WS_2-D_2	WS_2- Ar -D_2
Carbon	39.62	37.63	27.58	31.49
C-C	31.53	23.49	11.02	8.24
C-O	6.41	12.78	15.48	22.11
C=O	2.68	2.2	1.21	1.59
Oxygen (O1s)	7.82	10.69	10.17	10.95
Sulphur (S2p)	7.53	9.17	23.87	17.67
Tungsten (W4f)	3.55	4.04	10.66	7.95

Table S3: Comparison of the ratio between W^{+6}/W^{+4} and S-O/W^{+4}-O for pristine and plasma treated WS_2 NTs from XPS analysis.

	W^{+6}/W^{+4}	S-O/W^{+4}-O
WS_2	0.65	0.92
WS_2-Ar	1.41	1.54
WS_2-D_2	1.0	1.15
WS_2-Ar-D_2	1.08	1.33

Table S4: Electron paramagnetic resonance (EPR) values.

	g value	Hpp(G)Δ	Double Integration (DI) (a.u.)	Peak symmetry(A/B)
WS$_2$	2.003±0.003	7±2	74± 15	
WS$_2$-D$_2$	0.003±2.002	9±2	249±50	~1
WS$_2$-Ar-D$_2$	0.003±2.002	10±2	1506±300	~1

Table S5: Electrochemical performances. Values of resistances and capacitances obtained by EIS spectra in 0.5 M H$_2$SO$_4$.

	R$_s$ (Ohm)	R$_{ct}$ (Ohm)	CPE$_1$(μF)
WS$_2$	3.48	56.7	6.25
WS$_2$-Ar	2.71	15.01	8.08
WS$_2$-D$_2$	4.13	17.77	242
WS$_2$-Ar-D$_2$	2.78	13.21	7605

Interpretation. The equivalent circuit contains a resistor (R$_s$) connected with two parallel units in series: a constant phase element and a resistor (CPE$_1$-R$_{ct}$). The R$_s$ represents the solution resistance, the CPE$_1$- R$_{ct}$ pair is equivalent to resistor and capacitor in a parallel combination related to the charge transfer.
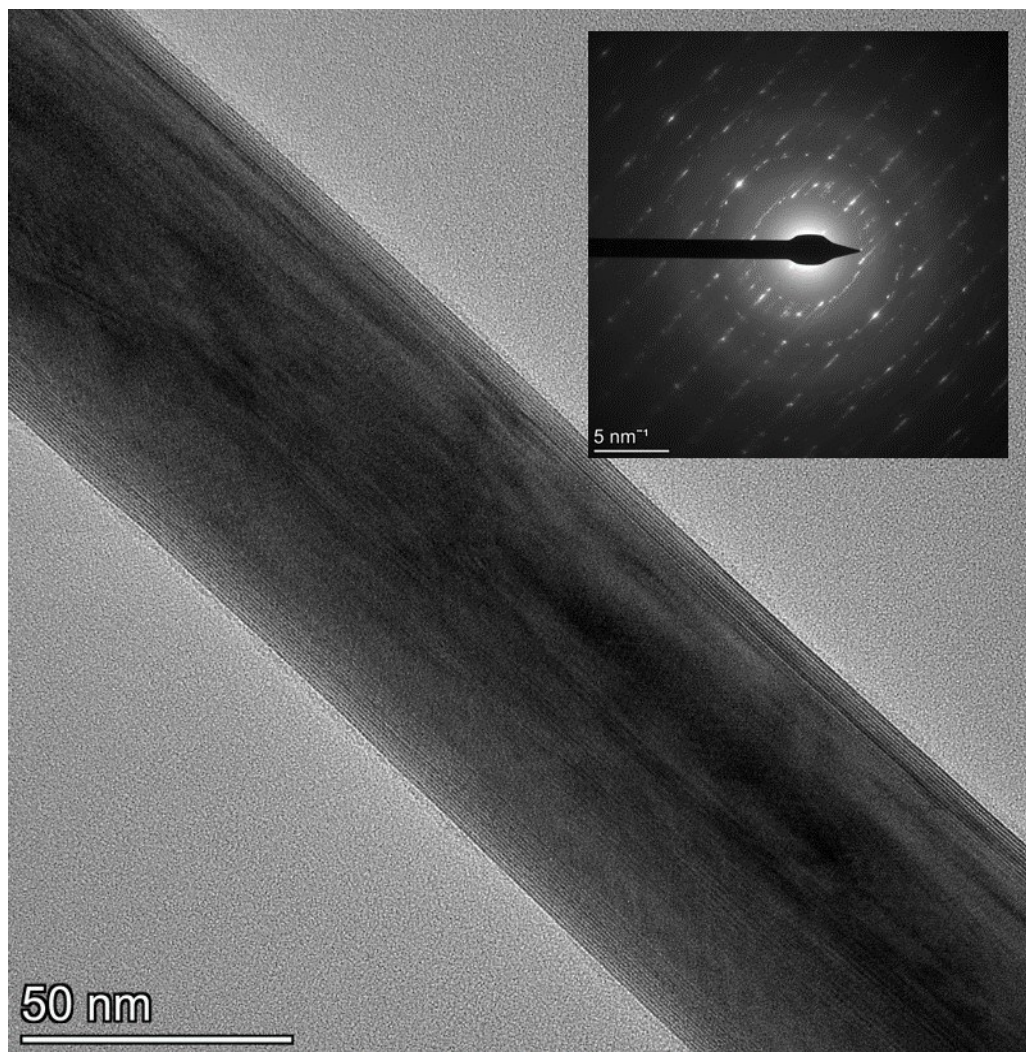
Figures

Figure S1. High-resolution TEM image of WS$_2$-Ar-D$_2$ NT confirms the retention of the multi-wall structure of the NTs. *Inset*: SEAD diffraction of the related area.
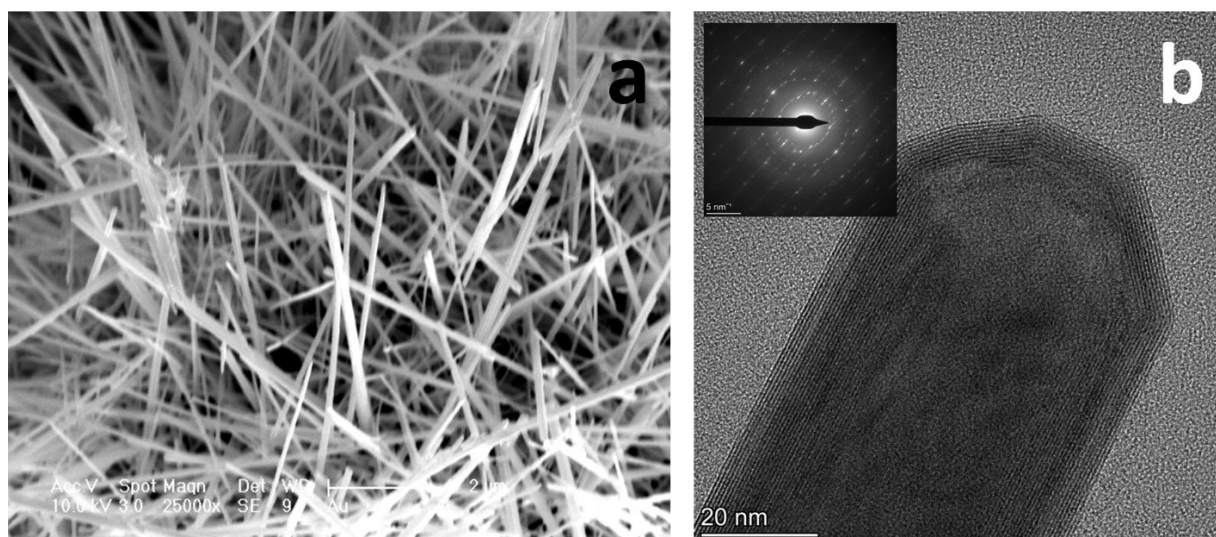
Figure S2. (a) SEM image illustrating the 1D morphology of the WS_2 NTs. (b) High-resolution TEM image of the pristine NT. A multi-layer pattern can be seen in the outer circumference of the NT wall. *Inset:* A selected area diffraction (SAED) designates the different WS_2 crystalline structure and 1D morphology.
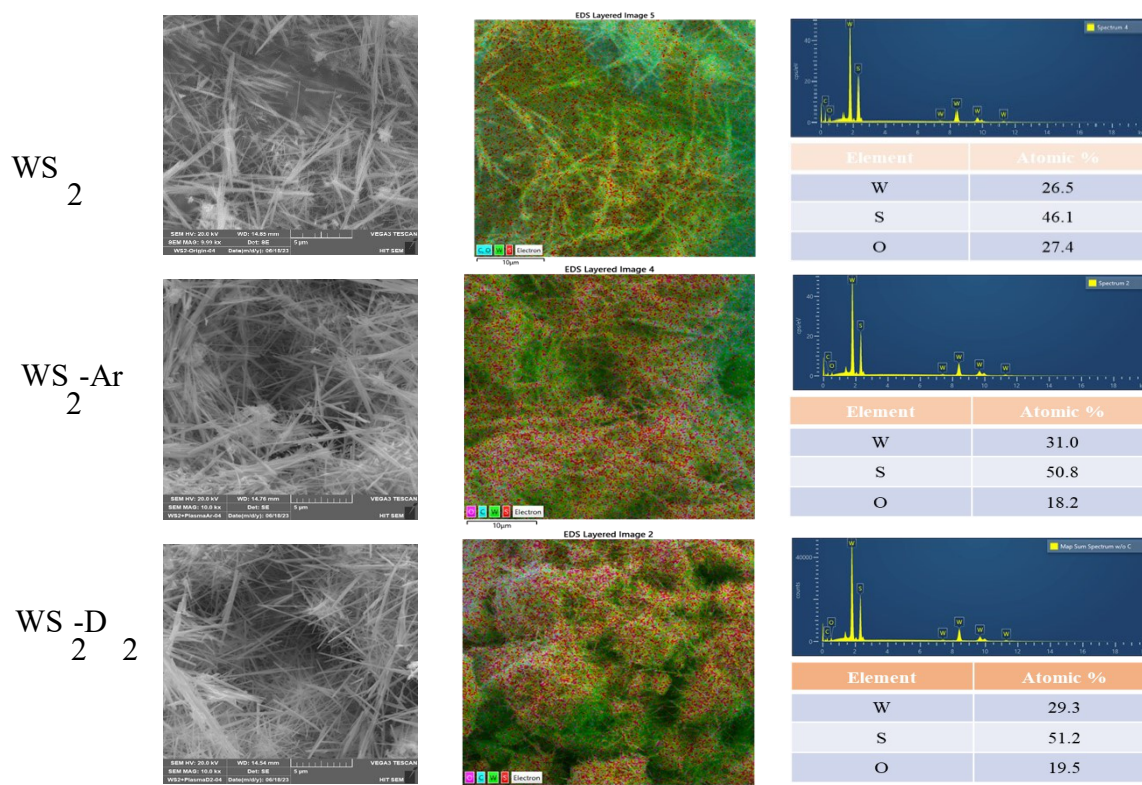
Figure S3. SEM images and corresponding elemental mapping by energy dispersive spectroscopy (EDS). The atomic percentages obtained by EDS are presented in the tables on the right.

Interpretation. The atomic W/S ratio for all samples is close to 1:2, with a slightly lower concentration of sulfur. This is a result of the WS_2 NTs synthesis process in which sulfurization starts from the surface of WO_{3-x} nanorods and continues inward. After this process some NTs did not undergo complete sulfurization (as described in the experimental section), and, therefore, contain some residual oxide in their core. The oxygen content after both Ar and D_2 plasmas is similar or a bit lower than in the pristine samples.
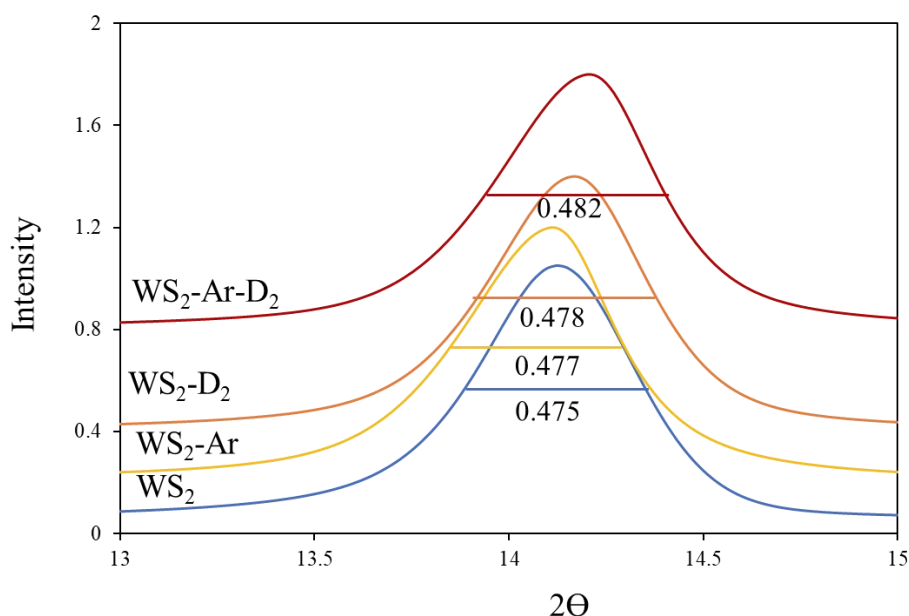
Figure S4: FWHM (Full-width half max) increases gradually from pristine WS_2 to subsequent plasma-treated samples.

Interpretation. The lattice parameters of WS_2, WO_2 and WO_3 are represented below:

WS_2: a = b = 0.315 nm, c = 1.227 nm, α = β = 90º, γ = 120°, Crystal System: Hexagonal.

WO_2: a = 0.321 nm, b = 0.484 nm, c = 0.576 nm, α = 90º, β = 123.48º, γ = 90°, Crystal System: Tetragonal.

WO_3: a= 0.531 nm, b = 0.521 nm, c = 0.769 nm, α = 90º, β = 91.50º, γ = 90°, Crystal System: Monoclinic.

Morphologic changes are observed in XRD. Bearing in mind the 1D morphology crystallization of WS_2 and, thus, overestimated intensity of (002) due to the preferred orientation, the broadening may have been the consequence of slight changes in the location and shape.

Peak shift. D-spacing shrinkage is possible when foreign +q ions intercalate between the layers; they can attract the layers, thus decreasing the d-spacing. Evidently, this happens only when D_2 is present in plasma due to the smaller size of D_2 molecules compared to Ar.

Peak broadening. While the Scherrer equation does embed a shape factor, it was not designed for 1D materials. Therefore, the results given in the supplementary may be considered purely indicative. Additionally, the crystallite size (the size of perfect lattice without defects) decreased from pristine WS_2 NTs to WS_2-Ar-D_2 NTs, indicating the plasma impact on the crystallization conditions. Determining the crystalline size according to the Scherrer equation shows a decrease of 3.4%.
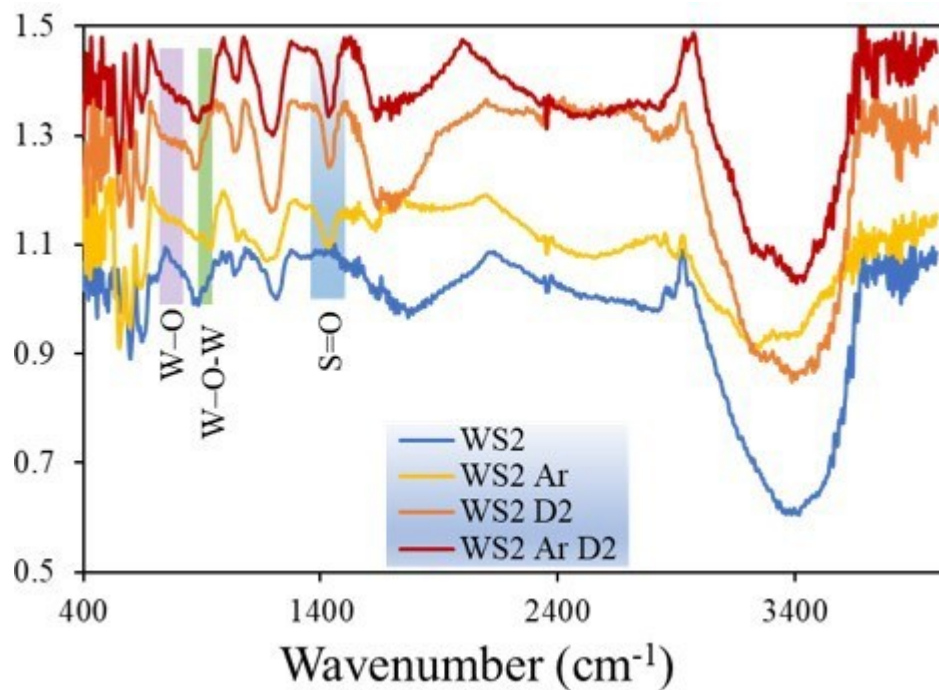
Figure S5. FTIR spectra of different WS_2 samples measured at broad wavenumbers corresponding to the data presented in Figure 1c.
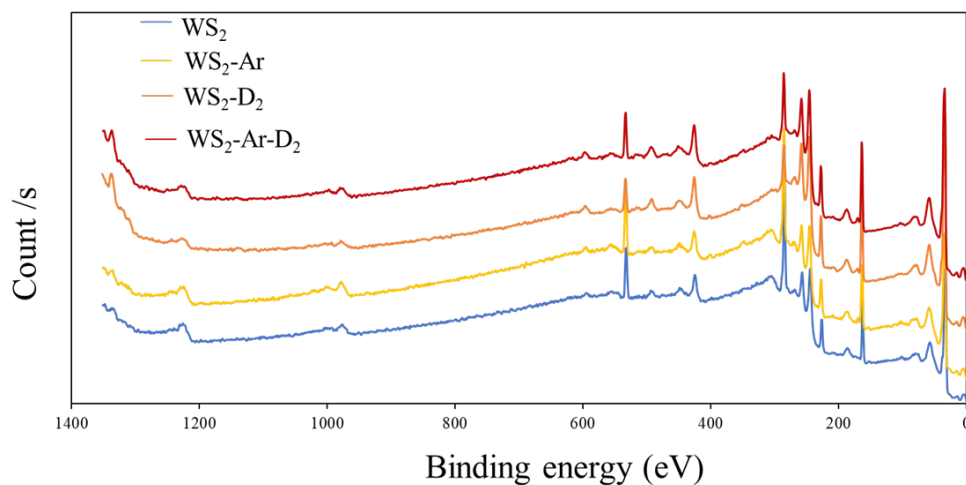

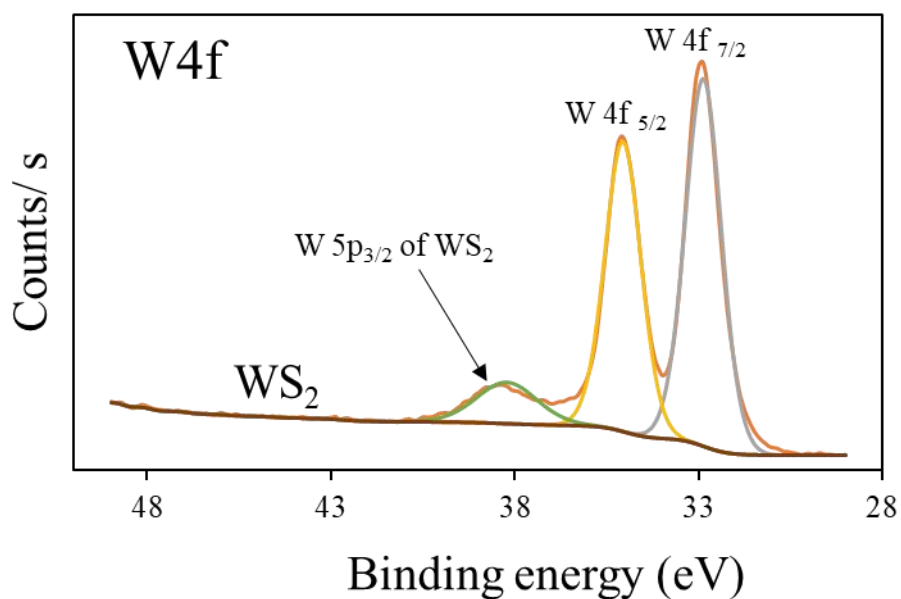Figure S6. Full XPS spectra of pristine WS_2 NTs and plasma-treated WS_2 NTs.

Figure S7. Deconvoluted W4f XPS spectrum of pristine WS$_2$ NTs. Binding energy is compared to the W4f spectrum of the plasma-treated samples that depicts peaks at a similar binding energy.
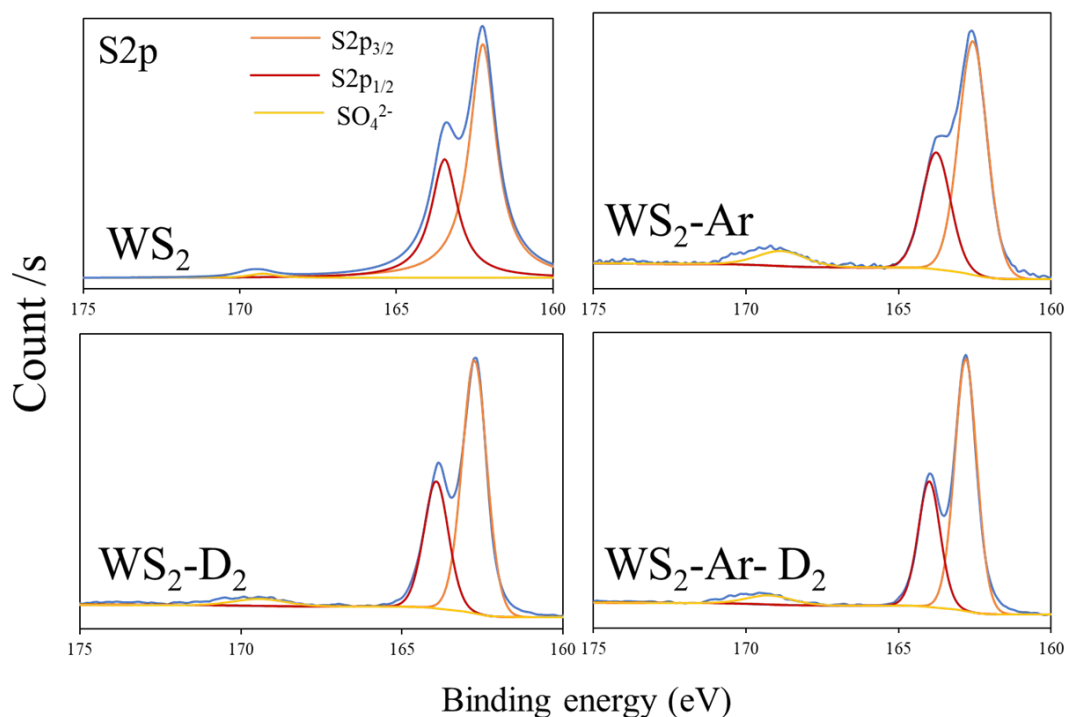

Figure S8. S2p XPS spectrum of WS$_2$, WS$_2$-Ar, WS$_2$-D$_2$ and WS$_2$-Ar-D$_2$ samples.

Interpretation. In the S2p spectra, two doublets are observed at 162.8 eV and 163.9 eV and attributed to the S2p$_{3/2}$ and S2p$_{1/2}$ of the divalent sulfide ions, respectively. The peaks at lower binding energies are related to the sulfur atoms (S-W bond) in WS$_2$ NTs, and the peaks at higher

energies (169.3 eV and 170.01 eV) attributed to S-O are due to surface oxidation. Both peaks are present in the pristine NTs as well. Thus, we can interpret that the S-O peak originates from natural oxidation by exposure to air. A small hump at a higher binding energy for each sample is related to the oxidized sulfate SO_4^{2-}.
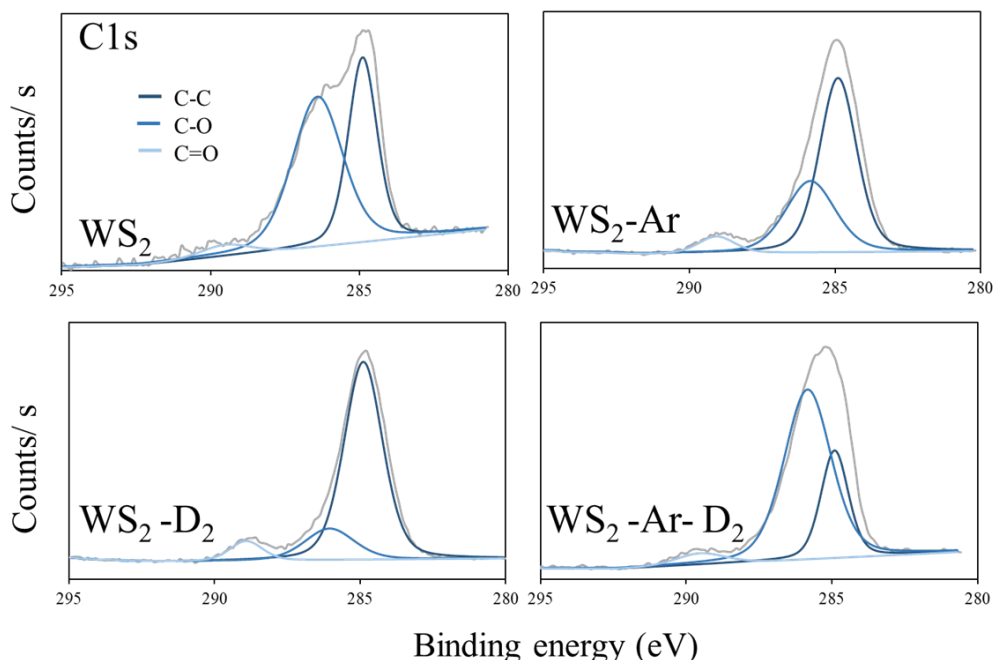

Figure S9: Deconvolution of C1s XPS spectrum of all plasma-treated and pristine NTs for different functional groups.

Interpretation. Carbon is not a primary element in WS_2 NTs; its appearance in XPS spectra is most probably a contamination. For the pristine WS_2 NTs sample, the amount of total C in atomic % is 39.62 %, which decreases to 37.62 % for WS_2-Ar, to 27.5 % for the WS_2-D_2 sample, and to 31.49 % for the WS_2-Ar-D_2 sample. As predicted, the amount of C-C bonds decreases from 31.53 % in pristine NTs to 8.24 % in the WS_2-Ar-D_2 sample, whereas the amount of C-O bonds increases from 6.41 % in the pristine sample to 22.11 % for the WS_2-Ar-D_2 sample. This significant loss of C-C bonds and an associated increase in the C-O bonds concentration eventually support the idea of surface oxidation following the plasma-induced treatment.
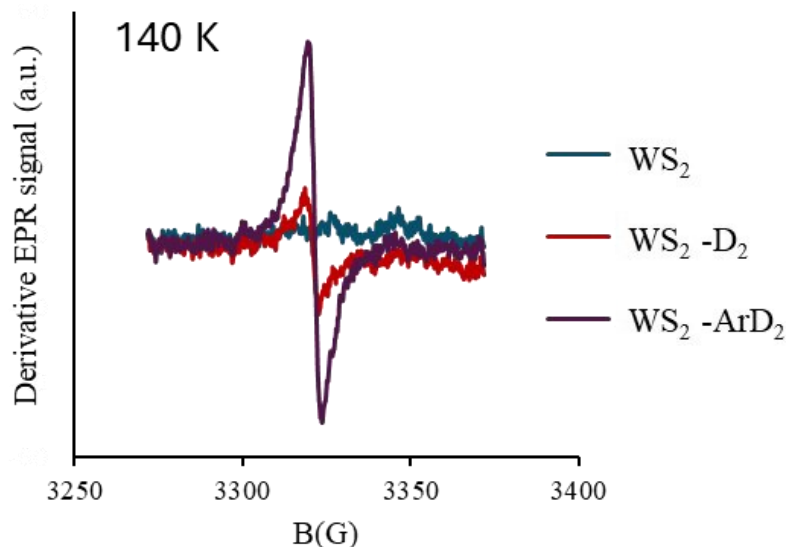
Figure S10. EPR signals of pristine WS_2, WS_2-D_2, and WS_2-Ar-D_2 NTs measured at 140 K.
Interpretation. The *g*-value is similar to that observed at the room temperature (Figure 3c). No EPR signal is observed for the pristine WS_2 NTs, while a clear signal is measured for the WS_2-D_2 sample. The EPR signal increased even more for the WS_2-Ar-D_2 sample. The significant EPR signal, even at 140 K, for the plasma-treated samples, proves the free radicals presence. Moreover, the fact that it is measured at such a low temperature indicates that the only possible origin of this signal is the formation of free electrons and not structural vibrations. Interestingly, the line width ΔHpp diverse from 9-10 G at room temperature to 4 G at 140 K. The small broadening of the peak at room temperature is probably caused by dynamics and motion at the room temperature, resulting in a *g*-strain and a Gaussian line shape as compared to almost Lorentzian line shape at 140 K.
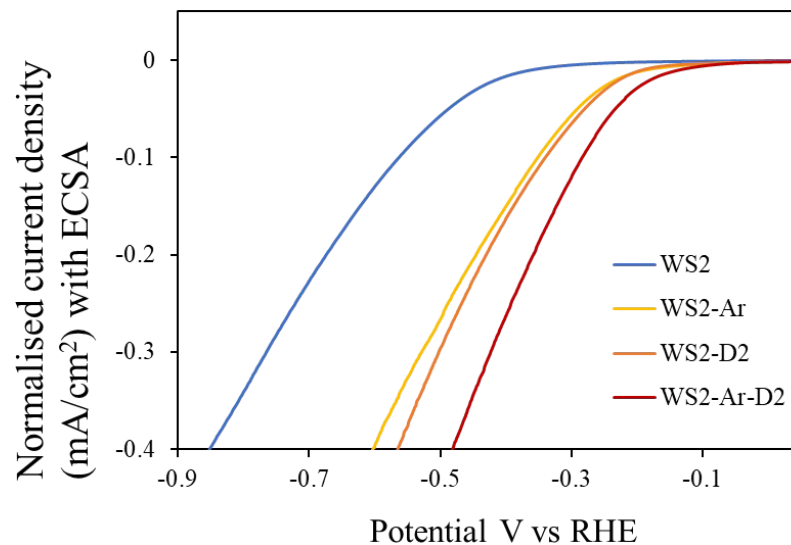
Figure S11: ECSA-normalized LSV curves showing better LSV performance for WS$_2$-Ar-D$_2$ catalysts compared to other plasma-treated and pristine WS$_2$ samples.
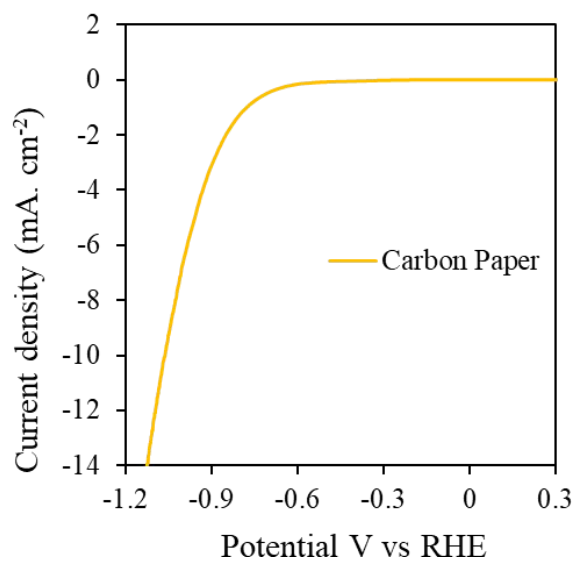

Figure S12: LSVs of the Toray carbon paper show its negligible effect on the catalytic performance.
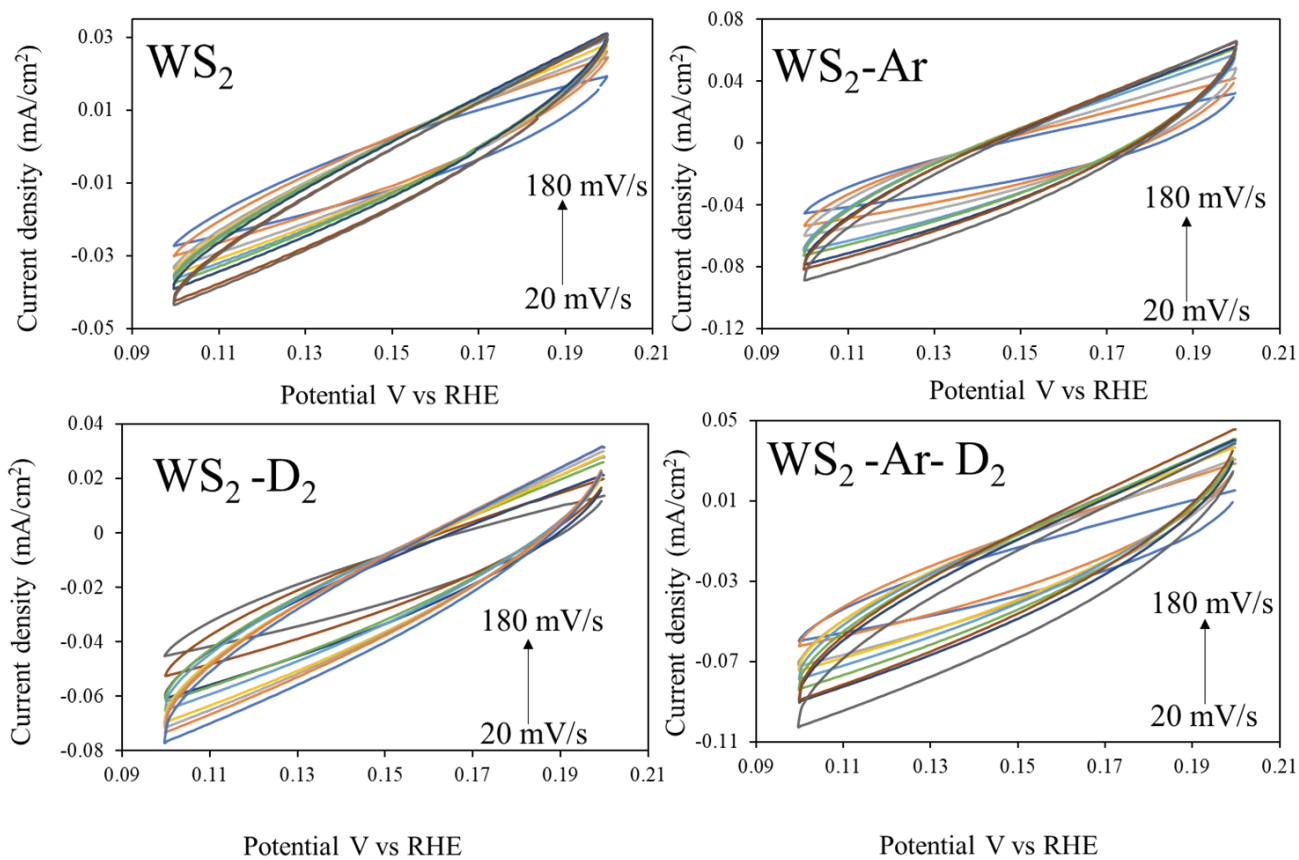
Figure S13: CV performances of WS2, WS2-Ar, WS2-D2, and WS2-Ar-D2 samples at different scan rates.